

Unfolding knots by proteasome-like systems: simulations of the behaviour of folded and neurotoxic proteins

Michał Wojciechowski* and Marek Cieplak†

Institute of Physics, Polish Academy of Sciences, Al. Lotników 32/46, PL-02668 Warsaw, Poland

Àngel Gómez-Sicilia* and Mariano Carrión-Vázquez

Instituto Cajal, Consejo Superior de Investigaciones Científicas,

(CSIC), Av. Doctor Arce, 37, 28002 Madrid, Spain and

Instituto Madrileño de Estudios Avanzados en Nanociencia (IMDEA-Nanociencia), C/ Faraday 9, 28049 Cantoblanco, Madrid, Spain

Knots in proteins have been proposed to resist proteasomal degradation. Ample evidence associates proteasomal degradation with neurodegeneration. One interesting possibility is that indeed knotted conformers stall this machinery leading to toxicity. However, although the proteasome is known to unfold mechanically its substrates, at present there are no experimental methods to emulate this particular traction geometry. Here, we consider several dynamical models of the proteasome in which the complex is represented by an effective potential with an added pulling force. This force is meant to induce translocation of a protein or a polypeptide into the catalytic chamber. The force is either constant or applied periodically. The translocated proteins are modelled in a coarse-grained fashion. We do comparative analysis of several knotted globular proteins and the transiently knotted polyglutamine tracts of length 60 alone and fused in exon 1 of the huntingtin protein. Huntingtin is associated with Huntington disease, a well-known genetically-determined neurodegenerative disease. We show that the presence of a knot hinders and sometimes even jams translocation. We demonstrate that the probability to do so depends on the protein, the model of the proteasome, the magnitude of the pulling force, and the choice of the pulled terminus. In any case, the net effect would be a hindrance in the proteasomal degradation process in the cell. This would then yield toxicity *via* two different mechanisms: one through toxic monomers compromising degradation and another by the formation of toxic oligomers. Our work paves the way to the mechanistic investigation of the mechanical unfolding of knotted structures by the proteasome and its relation to toxicity and disease.

Introduction

Neurodegenerative diseases are poorly understood and represent one of the major challenges to modern medicine [1]. Among these maladies, many are known to be tightly related to proteins that are present in the human brain. These proteins show similar traits. One is the tendency to form amyloid fibers within neurons and/or outside them [2, 3]. Another is the high mechanical polymorphism as assessed by single-molecule force spectroscopy [4] for polyglutamine tracts (polyQ, also denoted as Q_n , where n is the number of residues) as well as α -synuclein, β -amyloid, and Sup35NM. All of them are amyloidogenic intrinsically disordered proteins (IDPs) [4]. In equilibrium, IDPs may adopt a number of different conformations and interconvert in a nanosecond timescale [5].

The mechanical polymorphism of Q_n has been demonstrated to follow from a conformational one, which was characterized theoretically for n between 16 and 80 in ref. [6] by following the meta-dynamics methods used by Cossio *et al.* for polyvaline (polyV, denoted also as V_n) [7]. In particular, it has been found that about 9.3% of the 246 structurally independent Q_n conformers obtained for $n = 60$ were knotted compared to about 3.6% of the structures obtained for polyV of the same length [6].

It should be noted that some knotted structures can be spotted in the CATH database [8] which represents superfamilies of proteins as classified by their secondary structure motifs. We have checked that the previous version of CATH used for making comparisons in refs. [6] and [7] (5403 structures with the sequential length smaller than 250) contains 71 knotted proteins, smaller than 0.5%. The KnotProt database [9], devoted to proteins with knots, indicates that the smallest known knotted protein is MJ0366 from *Methanocaldococcus jannaschii* [10] – it comprises 87 residues, which is above the range of length considered in the Q_n systems in [6]. Its folding pathways have been studied in refs. [11–13].

One of the knots in the Q_{60} set [6] was of the three-twist (5_2) kind, with five intersections. Such a knot can be found in the Protein Data Bank (PDB) [14]. In particular, it is present in ubiquitin hydrolase UCH-L3 (PDB code 1XD3), a protein that deconjugates ubiquitin before degradation in the proteasome. Thus, the knot in this protein has been hypothesized to confer resistance to proteasomal unfolding [10]. All of the remaining knots identified in Q_{60} and all the ones found in V_{60} were of the common trefoil kind (3_1). No knots were found for n smaller than 35. Since the polyQ systems are IDPs, all the conformations, including the knotted ones, are transient. However, knots in polyQ last for hundreds of nanoseconds [6], two orders of magnitude longer than unknotted conformations. Properties of the globular knotted proteins are reviewed in refs. [15–17].

V_{60} is an artificial protein, in the sense that it cannot be found in nature. It was constructed to demonstrate that only a fraction of possible folds is adopted by proteins collected

*These authors contributed equally to this work.

†Electronic address: mc@ifpan.edu.pl

in the CATH database, implying a selective role of evolution, and perhaps also of physical constraints, in favouring certain folds [7]. This topic has been discussed for IDPs in ref. [18]. However, long polyQ tracts arise in nature near the N-terminus of several proteins, such as huntingtin, Atrophin-1 (ATN1), androgen receptor (AR) and several ataxins (ATXN). Huntingtin is known to be essential in embryonic development [19], and is considered to be related to gene expression regulation [20] as well as to anchoring or transport of vesicles [21].

Nonetheless, before translation, the genes encoding for these proteins contain long cytosine-adenine-guanine (CAG) repeats, which encode for the polyQ region. These CAG repeats are prone to due to slippage of the DNA polymerase [22] that elongates the number of CAG repeats in the gene and, therefore, the length of the polyQ tracts. If the length of the polyQ tract in the aforementioned proteins is greater than a (disease-dependent) threshold, they cause neurodegenerative diseases such as Huntington, dentatorubropallidoluysian atrophy (ATN1), spinal and bulbar muscular atrophy (AR) and many spinocerebellar ataxias (ATXN). Huntington disease, in particular, leads to progressive motor and cognitive impairments. The non-pathological length of the polyQ tract in huntingtin may start at 7 and is usually between 16 and 20 repeats [23], while the pathogenic threshold is around 35 residues.

The mutant huntingtin protein easily forms toxic oligomers and highly ordered amyloid fibers [24] and the toxicity of the oligomers may result from interactions with the membrane and perturbation of the calcium regulation [25, 26]. Nonetheless, other mechanisms point to toxicity appearing at different stages: either in the fibrillar state or at the monomeric level. In particular, a cell microinjection assay [27] has proved the toxicity of the monomers. The mechanisms of the monomeric toxicity can be related to the damage of the degradation machinery [4, 28]. Here, we propose that the toxicity may be due to the presence of knots in Q_n with n exceeding the disease threshold of about 35 – the typical sequential size, Δk , of a knot found in Q_{60} [6].

The knot-end locations are defined operationally through systematic cutting-away of the residues from both termini until the knot disintegrates [29, 30]. Location k_- denotes the end that is closer to the N-terminus and k_+ the one further away. The knots in Q_{60} are shallow since k_+ is always near the C-terminus, between sites 53 and 58, whereas k_- is between 16 and 23 [6]. Nonetheless, since the polyQ tract is close to the N-terminus of huntingtin, a knot in it would actually be deep. The evident lack of the N-to-C-termini symmetry reflects most likely the directionality of the peptide chain. Nevertheless the locations of the Q_{60} knot ends are seen to be much better defined and closer apart than those of the V_{60} ends [6].

For the sake of comparison with Q_{60} , we also consider four proteins that have a (non-transient) knot in their native state as they provide a well defined reference situation. Three of them are deeply knotted: the frequently studied methyltransferase YibK (PDB code 1J85 chain A, 156 residues) [10, 15, 31], RNA methyltransferase YBEA [17]

(1NS5 chain A, 153 residues), and ubiquitin hydrolase UCH-L3 [10] (1XD3 chain A, 229 residues). The fourth one, the just mentioned MJ0366 [17] (2EFV chain A, 82 residues), has a knot that is shallow. UCH-L3 contains a three-twist knot and the remaining proteins have trefoil knots. We shall use the PDB structure codes to refer to these proteins in a unified manner.

The relevance of the conformations with knots is that they may derail the degradation processes in the recycling machinery of the cell that are carried out by proteasomes, which would then lead to an increase in the concentration of the neurotoxic conformers. Derailing of the degradation machinery may occur either through a significant elongation of the degradation time or by an abandonment of the process only after a partial proteolysis. The idea that knotted globular proteins may disable proteasomes has been suggested by Virnau *et al.* [10] in the context of protein UCH-L3 but it has not been demonstrated. Here, we use a simplified model of the proteasome [32] and show that indeed jamming may take place both for the globular knotted proteins and for the transient knotted conformations in IDPs. We show that the degree to which the degradation is disabled depends on the protein, on its conformation, and on the terminus at which the intake into the proteasome starts. It also depends on the value of the effective pulling force of the molecular motor involved: the lower the force, the bigger the impediment. Whenever the probability of derailing the process of degradation is non-zero, an accumulation and aggregation of the toxic molecules would set in.

Although the term “proteasome” applies to the protein-degrading complexes in eukaryotes and archaea [33], we use it here in a general sense. In bacteria, examples of similar complexes are ClpXP and Lon proteases [34, 35]. The process of protein degradation is carried out in ATP-dependent proteases. All such proteases share a common shape: four stacked rings forming an axial channel and an inner catalytic chamber. We model the proteasome complex to be funnel-shaped and be endowed with impenetrable walls [32]. The funnel is composed of a torus that is fused together with a long cylinder as shown in the middle panel of Fig. 1. The detailed value of the geometrical parameters in our model are meant to render the structure of the proteasome derived in refs. [36, 37].

A proteasome operates as a molecular engine in that it attracts a (tagged) protein into its entrance and translocates it down its channel into the catalytic chamber where the protein is lysed into short peptides. In our model, the mechanical aspects of this action are mimicked by an application of a pulling force F_p whereas degradation itself is identified with translocation through a reference plane. An alternative and more detailed way to imitate the mechanics involved is to impose allosteric transformations in the proteins constituting the proteasome [38–40]. However, our simpler model has the advantage of accessing long time scales and generating a substantial number of trajectories that are necessary to statistically assess the role of the knotted structures. It also allows for a straightforward comparison with the situations in which the force is applied periodically, the pulling is performed at a constant speed, v_p , or when mechanical unfolding takes place without the proteasome. This simplified model does not de-

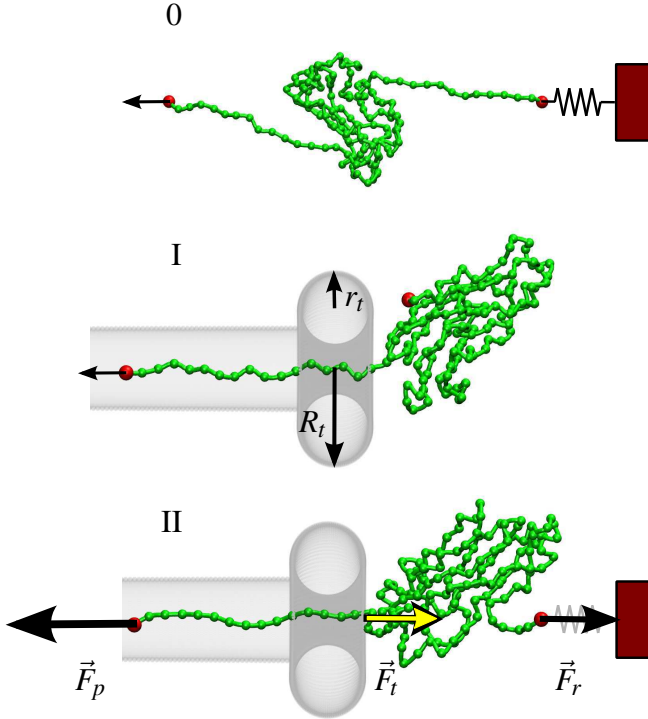


Figure 1: Protocols of pulling considered in the paper. Protocol 0 is the typical AFM-like pulling. Protocol I corresponds to the natural action of the proteasome. Protocol II is used in the measurements of the stalling force. The bottom panel defines the forces involved, as discussed in the text.

scribe the actual proteolysis nor the release of partially degraded proteins.

We have used this model [32] to characterize the nature of protein unfolding in the proteasome and to demonstrate that the stalling force measured by single-molecule force spectroscopy techniques [41, 42] may be smaller than the traction force of the unfoldase motor because one needs to include a mechanical reaction force, F_t , of the proteasome against which the protein is pushing, as shown schematically in Fig. 1 (bottom panel). Our model uses a simplified coarse-grained model of the protein [43–47] in which the amino acid residues are represented by effective atoms located at the positions of the α -C atoms and the solvent is implicit. The characteristic value of F_p is, as of yet, unknown. Nonetheless, it has been demonstrated [41] that degradation takes place at a rate of about 80 residues per second. Our approach in ref. [32] was to determine the characteristic time of translocation as a function of F_p and then to extrapolate it to the time corresponding to the degradation of the studied protein at the experimental rate. Here, we study properties as a function of F_p to get the sense of changes involved but do not actually extrapolate.

We consider three protocols of protein unfolding as illustrated in Fig. 1. Protocol 0 involves no proteasome: one terminus is attached to an anchored elastic spring while the other one is pulled. In protocol I, one terminus is dragged into the

proteasome and the other is free. Protocol II is similar, but the previously free terminus is attached to a spring which exerts a backward force, F_r . Pulling may be applied either to the N- or the C-terminus. The specific protocol used will be denoted as, for example, I-N and I-C respectively. It must be noted that obstruction for degradation in the I-N protocol does not imply an obstruction in the I-C protocol. The obstruction shows as jamming in our model and we shall use this term as a shorthand designation. In each of these protocols, pulling may take place in various modes. We consider the cases of a constant pulling speed, a constant pulling force and a force applied periodically. The last mode is the closest to how the proteasome actually operates since the process is controlled by the intermittent supply of the ATP molecules. Measurement of the stalling force has been done using mode II in experiments [41, 42].

Stalling occurs when the protein is unable to translocate. In the experiments performed in refs. [41, 42], this happened when the opposing force F_r is such that there is no translocation. We have argued [32] that F_r is not equal to F_p as commonly assumed, but to $F_p - F_t$ by the third law of mechanics. Here, we revise this issue and show that using an all-atom model of the protein combined with an explicit solvent also supports our previous finding about the interpretation of the measured stalling force. It should be noted that in our model, we separate all forces acting on the protein into two parts: the motor-like pulling and the reaction of the proteasome that resists the entry because of steric interactions. Our interpretation of the stalling experiments is that one measures the total force $F_p - F_t$ and not just F_p .

Materials and Methods

Our model of the proteasome has been introduced recently in ref. [32]. It assumes that the funnel-like geometry of the proteasome complex can be represented as an effective external potential, in analogy to several models of translocation through cylindrical channels [48–54]. The potential has axial symmetry, which reflects the fact that the two substructures of the biological proteasome – the 20S core particle, made out of four heptameric rings, and the two 19S regulatory caps – share an axial channel. The outer two rings of 19S caps form a gate where the polyubiquitin chains that are attached to the protein get recognized so that the protein is directed to the core chamber, leaving the chains behind (in the case of ClpXP, the proteins are tagged by short peptides at a terminus and the tags enter the proteolytic chamber).

The catalytic action takes place in the inner surface of the two rings in the middle of 20S. The target protein enters one of the caps and then moves further down the axial channel. The cap is represented by a torus and the channel by a cylinder. The channel is considered to be indefinitely long as we do not model the actual degradation. As a result, only one cap is included in the model and the protein cannot emerge “on the other side” and refold. The combined torus-cylinder shape defines the funnel.

The radius of the channel has been found experimentally

to be ≈ 7.5 Å [36, 37]. It is defined by the average distance between opposing heavy atoms on the inner side of the proteasome. We consider the channel to have a radius $r_c = 8$ Å to account for flexible adjustments of the channel. This channel is wide enough to accommodate a hydrated polypeptide and some elements of secondary structure. The torus is described by the equation $(x^2 + y^2 + z^2 + R_t^2 - r_t^2)^2 = 4R_t^2(x^2 + y^2)$, where the major radius is $R_t = 13$ Å and the minor radius is $r_t = 6$ Å. The opening in the narrowest place of the torus has a radius of 7 Å, which is smaller than the radius of the cylindrical channel describing the core particle. This disparity accounts for an extra cavity-like space that forms between the cap and the core particle.

In protocols I-C and I-N, the reference plane is defined as one shifted 25 Å inward with respect to the equatorial plane of the torus – where the opening in the funnel is the narrowest. The shift is introduced to make sure that the rear terminus is definitely within the cylinder. In protocol II, the criterion involved is arriving at an end-to-end extension which is equal to 85% of the backbone length. If a protein is knotted at the beginning, the evolution of the knot is followed during unfolding to check whether at the end it has tightened, untied or remained in place.

The interaction between the effective atoms of the protein and the surface of the torus as well as the inner surface of the cylindrical channel is assumed to be repulsive and given by the truncated Lennard-Jones (LJ) potential as follows

$$V_i^s = \begin{cases} 4\epsilon \left[\left(\frac{\sigma}{d_i} \right)^{12} - \left(\frac{\sigma}{d_i} \right)^6 \right] & , d_i \leq r_{min} \\ 0 & , d_i > r_{min} \end{cases} \quad (1)$$

where d_i is the smallest distance between the i th residue and the torus/channel surface. The distance $r_{min} = 6$ Å is the position of the minimum of the potential, which takes into account excluded volumes of residues and wall atoms. We take $\sigma = 0.5^{1/6} r_{min} = 5.345$ Å.

The energy parameter ϵ comes from our coarse-grained structure-based [55, 56] model of the substrate protein/peptide [43–47] – it is equal to the depth of the LJ potential associated with the contacts: $V_{ij}(r) = 4\epsilon \left[(\sigma_{ij}/r_{ij})^{12} - (\sigma_{ij}/r_{ij})^6 \right]$. The contacts are determined by using the criterion of atomic overlaps – the procedure denoted as OV in the detailed description of several approaches to the contact-map determination presented in ref. [57]. These contacts are only native in the case of globular proteins, whereas for the polyQ chains they are determined from the conformation at hand [6]. The value of the ϵ is approximately equal to 106 pN·Å, which correlates well with the experimental data on stretching at constant speed, after extrapolating to the speeds used in the experiments [47, 57, 58]. The length parameters σ_{ij} in the contact potentials are determined so that the potential minimum agrees with the native distances between i and j .

Bonded interactions are modelled by a harmonic potential with the spring constant of 50 $\epsilon/\text{Å}$. The local backbone stiffness is described by the chirality potential [46]. The solvent is represented by damping and random fluctuational forces, the amplitude of which depends on the temperature, T . Our sim-

ulations are performed at $k_B T = 0.3 \epsilon$ which is close to the optimal folding T of the model proteins [44] (k_B is the Boltzmann constant). With our calibration of ϵ this choice is also consistent with studies performed in a vicinity of the room temperature. The time unit, τ , in the simulations is of order 1 ns due to overdamping.

The initial placement of the protein/polypeptide relative to the proteasome model is based on the following procedure. Both termini are located on the main axis of the proteasome and away from the torus. The protein is then moved towards the torus in small steps until one of the heavy atoms collides with it. The placement just before this last step is taken as the starting state. Henceforth, in the coarse-grained model, only the α -C representation is used dynamically. The coordinate reference system is chosen so that the central axis of the cylinder is along the z axis. In protocol I, translocation is said to take place if all of the system moves past the reference plane defined before. The time needed to accomplish this defines the translocation time, t_T . In protocol II, the characteristic time corresponds to achieving a nearly full extension (85%).

In the part where polyQ is considered, the structures are taken from [6]. HTT, which stands here for the exon 1 of huntingtin, was obtained by homology modelling using MODELLER [59]. Knotted and unknotted HTT are based on two templates: The structured regions were taken from the X-Ray-resolved 17-glutamine structure under the PDB code 3IOR [60], while the (knotted or unknotted) polyQ from ref. [6] were used as templates for the polyQ region. 10 models were done for each conformation, each one was checked to preserve the knotting state (HTT must be knotted if polyQ was knotted and *vice versa*) and the lowest-energy configuration from those was chosen to stretch.

In the final part of this work, we consider an unknotted protein which represents a model protein in the field of single-molecule force spectroscopy, the I27 domain of cardiac titin whose PDB structure code is 1TIT and which has a net charge of $-6 e$. We reexamine the issue of the stalling force – now by using all-atom simulations. These simulations were performed by using the GROMACS 4.6.5 package [61] with the AMBER99 force field [62]. The molecules of water are described within the TIP3P model [63]. The time integration of the equations of motion was performed using the leap-frog algorithm with a time step of 1 fs. We have added 64 Na^+ and 58 Cl^- ions to neutralize the system and to keep the nearly physiological ionic strength of 150 mM. The GROMACS-based model was augmented with the potential due to the proteasome walls (eq. 1) constructed in the same fashion as in the coarse-grained simulations except that now the cylinder needs to have a finite length. The system was placed within a cuboid box with the extension of 100 Å in the x and y directions and 200 Å in the z direction. The long direction of the cuboid coincided with the central axis of the proteasome model and the equatorial plane of the torus is 135 Å away from the bottom of the system. Periodic boundary conditions were used.

The water molecules are allowed to be above the plane corresponding to the top of the torus and within the inside of the proteasome model. Due to the periodic boundary conditions,

the water molecules can also be at the bottom of the cuboid box, *i. e.* underneath the end of the cylinder (which has a finite length in all-atom simulations). There are also two repulsive walls so that the cylinder is not surrounded by water. One is at the bottom of the cylinder (at 7 Å above the bottom of the whole system) and another at the top of the torus (away from the center). The equilibration of water in the initial stage was implemented through 1 ns while holding the protein frozen in its native state.

When determining the forces of interactions with the proteasome walls, all the atoms of the protein and water are considered as having a radius of 2 Å and the wall itself is thought of as being made of atoms also with a radius of 2 Å. A purely repulsive potential for interactions with the wall of the funnel leads to an expulsion of water from the proteasome model (without affecting the protein). In order to hold the water in, we consider a modified attractive LJ potential – augmented by the term $A/r + B$ – where the parameters A and B were selected so that both the force and the potential vanish at 7 Å (slightly smaller than the radius of the cylinder). The energy parameter was taken to be 4 kJ/mol. It should be noted that this value is an order of magnitude larger than, say, the C–C energy parameter in the AMBER99 force field, 0.359824 kJ/mol. The reason for this resides in the fact that the cylinder has no atomic structure and larger values are needed. VMD [64] has been used for the representation of protein structures.

Results

Constant velocity

There is no constant speed pulling in real proteasomes. However, this mode of action allows one to derive a characteristic force which is also of relevance for constant force situations as it approximately corresponds to a crossover between the low and high force behaviors [65]. Consideration of the constant speed processes also sheds light on possible hindrances to translocation and allows for a direct comparison to typical constant-velocity experiments in atomic force microscopy (AFM).

At constant v_p , one monitors the tension, F , in the backbone and studies it as a function of the displacement, d , of the spring that is attached to the pulled end of the protein. The characteristic force, F_{max} , associated with a protein is defined as the height of the maximal isolated force peak. It depends on v_p in a weak way (approximately logarithmically) so one may state that F_{max} refers to a certain narrow range of relevant forces. We take v_p to be $0.005 \text{ Å}/\tau$, which is typically two orders of magnitude faster than in the AFM experiments (in the absence of a proteasome).

In addition to determining $F(d)$, we monitor the time dependence of the sequential location of the knot ends. When pulled without the proteasome, the knot ends have been discovered to jump to preferred locations [66], instead of moving in a diffusive manner, until getting tightened maximally.

Fig. 2 provides an illustration of the $F(d)$ plots for 1J85 obtained in the five protocols of pulling. We have consid-

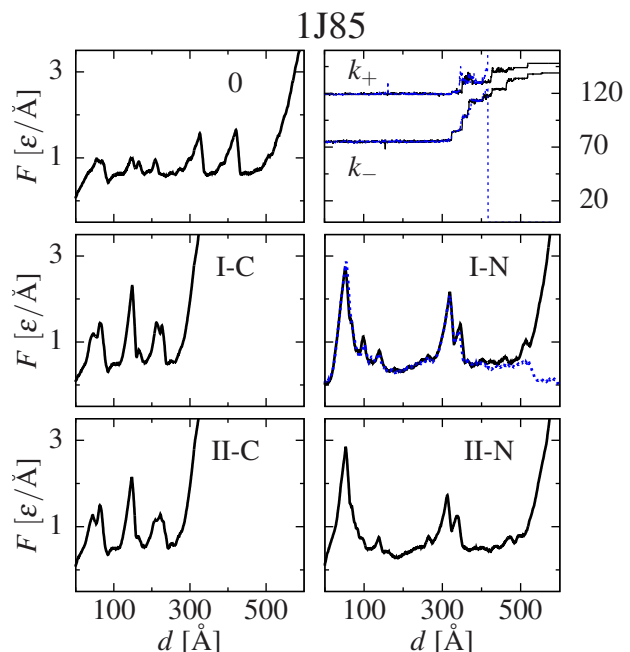


Figure 2: Example F – d recordings for 1J85 in the different pulling protocols at a constant speed. The top-right panel shows the locations of the knot ends in protocol I–N for two trajectories. In one trajectory (dotted blue lines), the knot unties and the protein translocates. In the other (solid black lines), the protein jams the channel and the tightened knot arrives at a permanent location. The profiles have been selected out of 100 trajectories for each protocol. The profiles shown in the middle-right panel correspond to the trajectories shown in the top-right panel.

ered 100 trajectories. For the I–N protocol about 50% of the trajectories lead to jamming combined with the tightening of the knot. The motion of the knot ends along the sequence is shown in the top-right panel of Fig. 2. The remaining 50% lead to translocation, as shown in the left panels of Fig. 3, combined with untying of the knots in which the knot ends move to the termini, which means that the knot disappears. In all other protocols, all trajectories lead to jamming in which the knot may or may not change location. Typically, jamming involves the knot being unable to enter the cylindrical channel.

The $F(d)$ patterns are seen to be visibly affected by the presence of the proteasome and, in particular, the values of F_{max} are generally different than those in protocol 0. Note that stretching in protocol 0 invariably leads to knot tightening whereas the action of the proteasome model may also lead to the knot slipping off the backbone, especially if the knot is shallow. It is interesting to note that knotted proteins pulled by the proteasome have F_{max} larger than in its absence. On averaging over the trajectories, for 1J85 we get $\langle F_{max} \rangle$ of 1.85, 2.67, 3.13, 2.48, and 3.09 $\epsilon/\text{Å}$ for protocols 0, I–C, I–N, II–C, and II–N respectively. For 1NS5, the corresponding numbers are 1.97, 2.71, 2.50, 2.42 and 2.69 $\epsilon/\text{Å}$.

In the case of 1NS5 (see S1 Fig.), protocols I–C and II–C may lead either to translocation or to jamming whereas protocol II–N leads only to jamming. For protocol I–N, only about

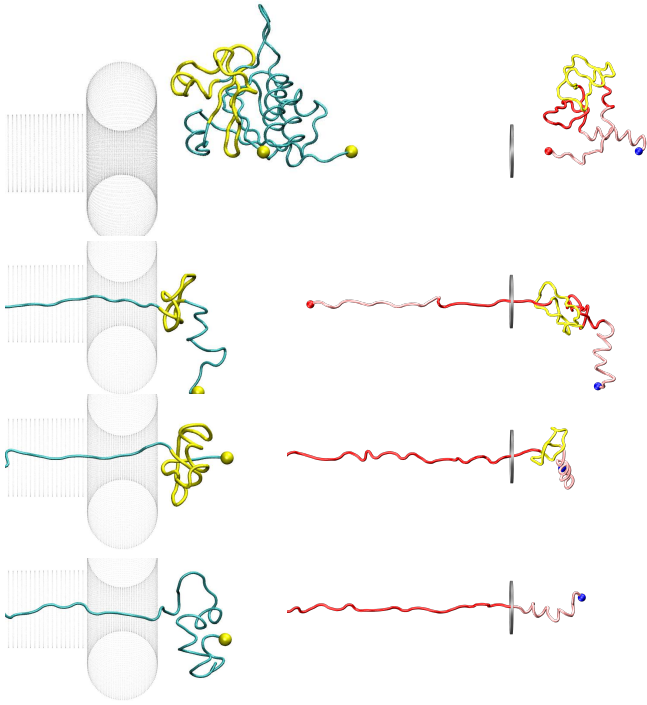


Figure 3: Two example trajectories that lead to translocation of knotted species. The left panels show translocation of 1J85 when pulled in the I-N protocol and the right ones the unfolding of a HTT_{60} knotted conformation. The knot is marked with yellow. In the case of HTT_{60} , the polyQ part is marked in red.

4% of the trajectories end up in translocation. The knot is located near the C-terminus so one would expect that it unties readily during pulling by the N-terminus; however, the opposite is observed. In the case of 1XD3 (see S2 Fig.), almost all I-C and II-C trajectories lead to translocation. For I-N, 35% trajectories unfold and for II-N – none. The values of $\langle F_{\max} \rangle$ exceed or equal (in the case of protocol II-N) the $\langle F_{\max} \rangle$ for protocol 0. For the shallowly knotted 2EFV (see S3 Fig.), $\langle F_{\max} \rangle$ in protocols I and II is close to that in protocol 0 (within $0.1 \text{ } \epsilon/\text{\AA}$). The knot easily unties in protocols I-N and I-C and translocation is unhindered. However, in protocol II-C, there is no instance of translocation whereas in II-N translocation occurs with a probability of 30%. The knot ends are at sites 11 and 73 (the full length of the protein is 87, but the structure of the first five residues is unknown and therefore the model does not include them).

We conclude that keeping the backward terminus supported, as in the experiments on the stalling force, affects the physical outcome of the process. For instance protein 2EFV translocates in protocol I-C but it does not in protocol II-C. Also, protocol II precludes untying of knots.

We now consider the constant velocity pulling of Q_{20} and Q_{60} , below and above the pathological threshold, respectively, of most polyQ-related diseases including Huntington. Using the conformations obtained in ref. [6], we study the degradation of these proteins using protocols 0 and I-C. We focus on the C-terminus because polyQ and exon 1 of HTT are close to

the N-terminus, so pulling from the N-terminus is expected to be less favorable in comparison. The left panels of Fig. 4 show the probability of unfolding at force F_{\max} comparing both protocols. Remarkably, the modal mechanical stability of Q_{20} is significantly larger in an AFM-like scenario (protocol 0, solid black) than when translocated through the proteasome (protocol I-C, dashed red). On the other hand, the distribution of mechanical stabilities for Q_{60} in the proteasome is shifted to the right and the number of non-mechanostable conformations ($F_{\max} = 0$) is significantly lower than the case of the AFM-like pulling. This already suggests that pathological polyQ tracts are harder to degrade than non-pathological ones.

S4 Fig. shows that there is no statistical relation between the mechanical stability when measured by protocols 0 and I, as already explored in ref. [32] for globular proteins. Furthermore, knotted conformations are not clustered, but scattered and essentially indistinguishable from the rest of the structures. Interestingly, two of the knotted conformations show no force peaks in protocol 0 but have a high force in the proteasome ($F_{\max} \approx 1.8 \text{ } \epsilon/\text{\AA}$), in accordance with the results for globular knotted proteins.

We studied each of the Q_{60} knotted conformations from ref. [6] by translocating them through the proteasome at a constant speed 20 times each. Most of the knotted conformations translocate always, resulting only in a 7% of jamming.

Upon the addition of the handles of HTT exon 1 to the knotted conformations, nonetheless, there is a significant change in the behaviour: jamming increases to an 11%. The success rate in this case is then reduced to 89%. Examples of jamming and translocation can be observed as force–extension plots in the middle panes of Fig. 4. The right panels of this figure show differences between pulling simply the polyQ region (Q_{60}) or the whole exon 1 of huntingtin (HTT_{60}). The mechanical stabilities also show a significant shift: even though the fraction of non-mechanostable conformations is similar, the distribution of forces for HTT_{60} is significantly shifted to the left, which implies that smaller forces are needed in order to unfold it than those needed for Q_{60} . Nonetheless, some structures show a large increase in the force, reaching mechanical stabilities as high as $3.5 \text{ } \epsilon/\text{\AA}$. Interestingly, no correlation is observed between the mechanical stability of HTT_{60} and Q_{60} , suggesting that the handles may play a very important role modulating this property.

Constant force

The processes at constant F_p are described by plots of the end-to-end distance, L , as a function of time, t , for individual trajectories and by determining the associated characteristic success time. For protocols 0 and II, we define success to be the unfolding of 85% of the full backbone length (when few, if any, contacts are left) and the characteristic time is denoted by t_U . For protocol I, it is the translocation time t_T . The native values of L are 20.1, 22.0, 37.6, and 36.0 \AA for 1J85, 1NS5, 1XD3, and 2EFV respectively.

Fig. 5 shows examples of the trajectories for 1J85 obtained under protocol I-C. We observe no events of transloca-

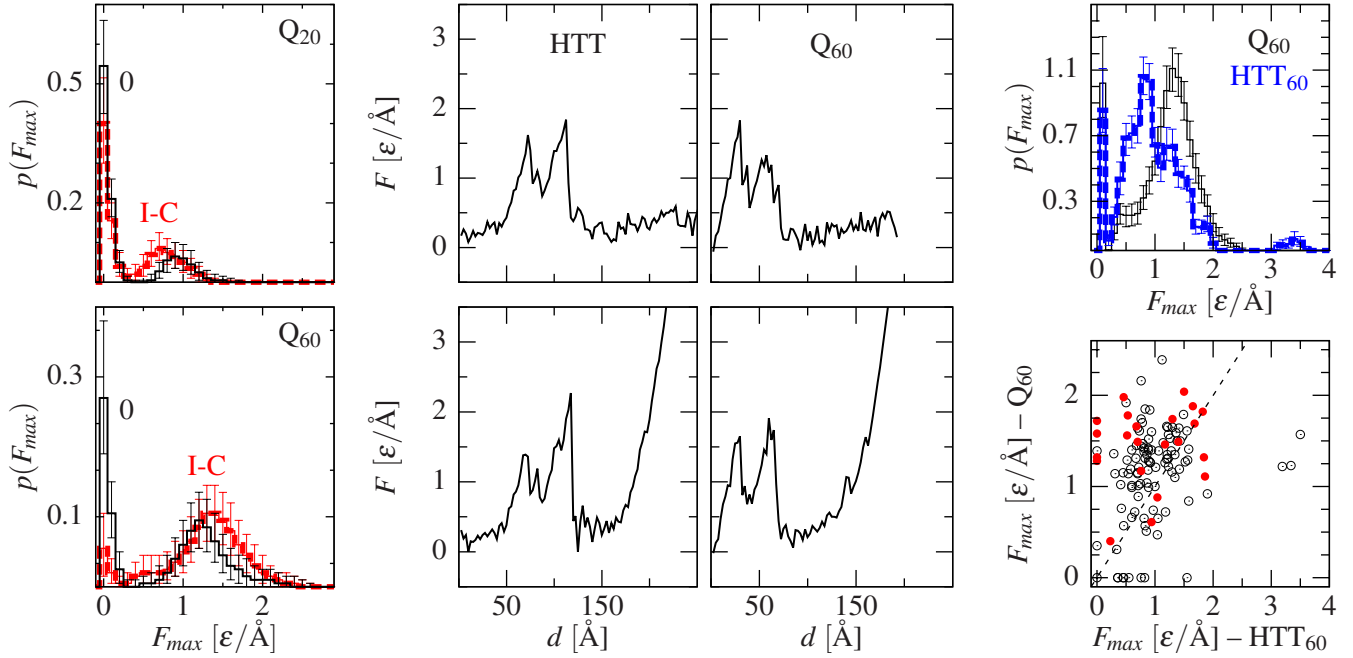


Figure 4: Constant velocity pulling analysis of polyQ. The left panels show a distribution of mechanical stabilities for the Q_{20} and Q_{60} conformations when pulled in protocol 0 or I-C. The two middle panels show examples of F - d recordings of the proteasomal unfolding – protocol I-C – of knotted HTT (left) and Q_{60} (right) molecules that translocate (top) or induce jamming (bottom). All panels correspond to the same starting conformation, thus the similarity in the unfolding pattern. The right panels compare the mechanical stability of Q_{60} with and without the exon 1 handles of huntingtin. The former is called HTT_{60} . The top panel shows the distribution of mechanical stabilities, while the bottom panel shows a scatter plot comparing the mechanical stabilities in each of the cases, with the knotted conformations highlighted in red. In this analysis, $F_{max} = 0$ means there is no articulated force peak greater than the thermal noise ($0.1 \text{ } \epsilon/\text{\AA}$) in the force–extension plot. The error bars in the histograms represent a 95% confidence interval.

tion, similar to the constant velocity simulations (between 10 and 20 trajectories were generated for each F_p in this case). For $F_p \leq 1.6 \text{ } \epsilon/\text{\AA}$ and for most (90%) of the trajectories for $1.7 \text{ } \epsilon/\text{\AA}$ the knot stays at its native location as illustrated in the left panel of the figure. On the other hand, in all trajectories with $F_p \geq 1.9 \text{ } \epsilon/\text{\AA}$ and 45% for $1.8 \text{ } \epsilon/\text{\AA}$ the knot gets tightened – both knot ends move to nearly the same locations. The tightened knot may partially enter the channel of the proteasome model. Similar results were obtained for 1NS5 in protocols I-C and I-N, shown in S5 Fig.: the knot may get tightened but there is no translocation. We conclude that knots form an insurmountable hindrance to translocation of the deeply knotted proteins if pulling is performed under the conditions of constant force.

Similarly, we have also studied Q_{60} under a constant force unfolding in the I-C configuration at different forces, and compared it to HTT_{60} . As observed in constant velocity pulling, knotted conformations are sometimes unable to translocate through the proteasome, leading to stalling. Right panels of Fig. 3 show snapshots of the translocation of one of the HTT molecules, up to the untying of the knot.

The top panel of Fig. 6 shows the translocation time as a function of the force for Q_{60} comparing unknotted conformations to knotted ones. The former show a typical two-state curve for the force dependence whereby t_T depends on the force exponentially in two regimes. The knotted conforma-

tions, however, show an optimal F_p for translocation around $2 \text{ } \epsilon/\text{\AA}$. Forces below this value take longer to untie the knot, while forces above tend to stall the proteasome, so they take much longer to translocate.

The bottom panel of Fig. 6 shows the probability of the molecule not being able to translocate in the simulation time ($10^7 \tau$), which we operationally define as a stalling of the proteasome. We can see that even if the translocation is not always achieved at low forces, there is a significant difference between the stalling of the proteasome due to knots and that due to other mechanical elements such as the typical shearing mechanical clamps proposed in [4].

Finally, the comparison of the isolated Q_{60} to the one with exon 1 handles, HTT_{60} , shows that the translocation time grows, as expected by its longer sequence, while the stalling is similar at high forces. Interestingly, the N-terminal tail facilitates the unknotting at low forces, so that the stalling is reduced – compared to the isolated polyQ – and is comparable to the unknotted peptides. Furthermore, since it was proposed [4] that proteasomal jamming might be induced by highly mechanostable conformations (called hM in ref. [4]), we also compare the translocation time of the conformations that, in protocol 0, have $F_{max} > 1.5 \text{ } \epsilon/\text{\AA}$. Indeed, the results shown in Fig. 6 show a significant difference between this subgroup and the whole set, but the effect due to knots is much greater.

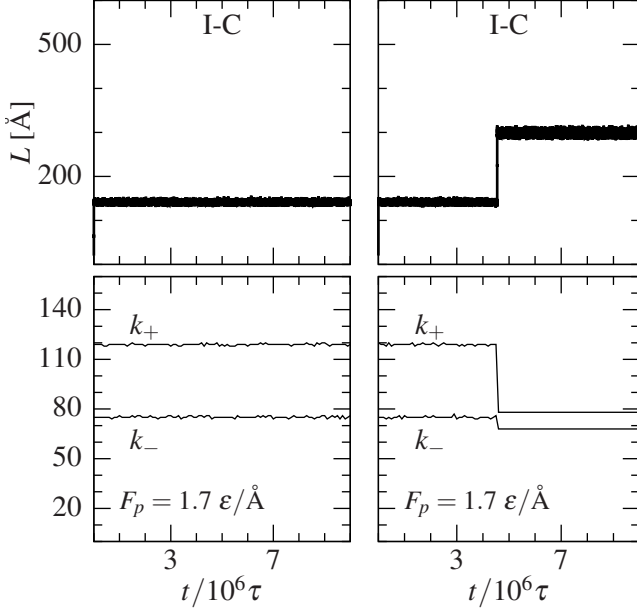


Figure 5: Examples of constant force trajectories for 1J85 in the I-C protocol for $F_p = 1.7 \text{ } \epsilon/\text{\AA}$. Two situations arise for this protein: The knot ends remain static (left) or the knot tightens (right), but translocation is never achieved.

Regarding the shorter polyQ chains, Q₄₀, our previous study [6] did not generate conformations with knots – most likely because of an insufficient statistics. Nonetheless, Q₄₀ is above the threshold of most polyglutaminopathies (~ 35) and above the minimal sequential extension of the trefoil knot. Thus, the presence of knots in Q₄₀ should provide hindrance to translocation like in the case of Q₆₀. In order to model this effect, we generated knotted Q₄₀ conformations by making use of the knotted conformations of length 60 and then by pruning the sequence at both ends in such a way that the total length becomes 40 residues while the knot becomes centered (the number of the residues from k_- to N is the same as the number of residues from k_+ to C. S6 Fig. shows that the behavior of these constructed knots is similar to the knotted subset of Q₆₀ at the relevant regime of smaller forces while is slightly different at higher forces.

Taken together, our results reinforce the hypothesis of the knots being responsible for the malfunctioning of the degradation machinery, at least in polyQ-related diseases, even if the degradation is stalled for shorter times.

Periodic force

We now consider a situation in which the force is applied periodically: for half of the period the force is F_p while for the other half the force is zero. We take the period to be 9000τ .

Fig. 7 shows two examples of translocating trajectories for 1NS5 in protocol I-C at $F_p = 1.8 \text{ } \epsilon/\text{\AA}$. In the initial stages of

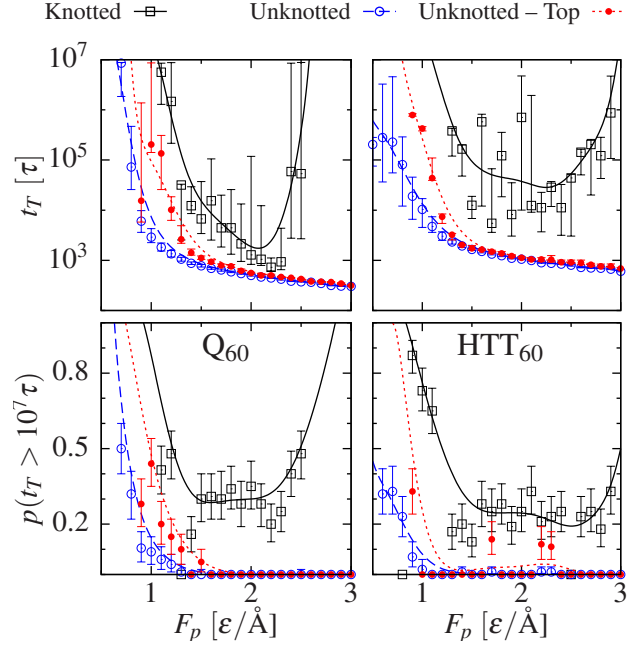


Figure 6: Comparison of the translocation time (top) and stalling probability (bottom) of the knotted and unknotted Q₆₀ (left) and HTT₆₀ (right) as a function of F_p . The stalling probability is defined as the probability of the protein taking longer than $10^7 \tau$ to translocate. Each point corresponds to the median value, and the error bars represent a 95% confidence interval. It can be observed that knotted conformers (solid black line) take longer to translocate than unknotted ones (dashed blue line) and stall with a higher probability. Furthermore, even though mechanical stability does not relate to translocation time, the top- F_{max} species (called “Unknotted-Top”, dotted red line) translocate slower and stall more often than the average unknotted ones, although less often than knotted. The tendency at lower forces for both knotted and top- F_{max} conformations is to stall the proteasome, so both could in principle be responsible for the malfunctioning of the proteasome. In this case, the knots are expected to be more troublesome, since they last for tenths of microseconds [6] as opposed to nanoseconds [5].

the process, L gets extended but then returns to the near-native value in the second idle part of the periods. After a number of attempts, a substantially longer extension arises and the return to the native situation is no longer possible. Eventually, the translocation is accomplished.

For a set of 100 trajectories, all are observed to lead to translocation at this F_p and to involve untying of the knot. The median t_T is $56\,270 \tau$. On lowering the force, the median t_T grows (the solid line in the top panel of Fig. 8) as does the number of instances in which the protein is stuck at the entrance with its knot ends fixed at their native values (69 and 119). For an F_p of $1.40 \text{ } \epsilon/\text{\AA}$, the odds of a successful translocation become equal to jamming, at least within the cutoff time of $10^7 \tau$. The shortest median t_T is for an F_p of $2.2 \text{ } \epsilon/\text{\AA}$. It increases to about $90\,000 \tau$ at $3.0 \text{ } \epsilon/\text{\AA}$ (which is hard to see in the scale of the figure).

The periodic modulation of the pulling force imitates the

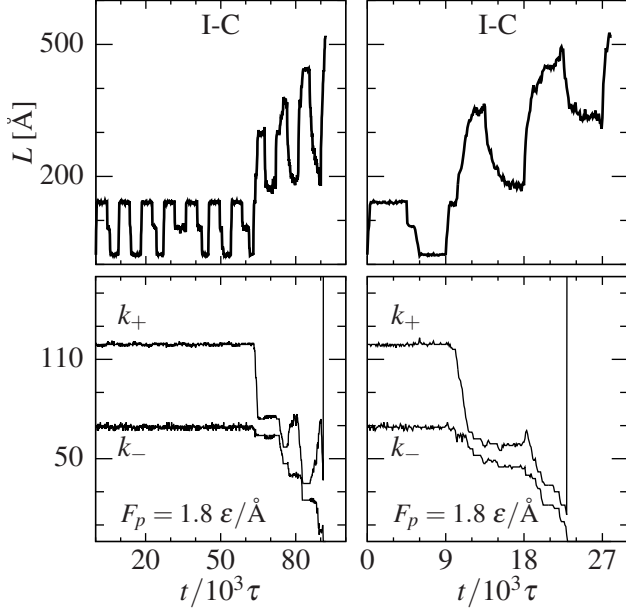


Figure 7: Examples of trajectories for 1NS5 with the pulling force applied periodically. After each period of pulling, the protein may either retract (six instances of retraction to the near native situation in the left panels and one in the right panels) or stay in an extended state.

periodic processing of the ATP molecules to the proteasome. However, the exiting back out of the proteasome does not seem to be observed experimentally [41]. In order to remedy it, we consider a ratchet-like model in which the acceptable advancement during one half-period is up to 3.8 Å . In the remaining part of the period, the protein in the channel is held fixed by a harmonic spring at the pulling end while the outside portion of the protein may equilibrate. The spring constant, k_z , used in the ratchet mechanism is weak and is set to be equal to 2 ε/Å^2 . In order to set the reference location z_{ref} , we monitor the z -coordinate of the most forward residue. This provides the initial value of z_{ref} . If the residue moves by 3.8 Å with respect to z_{ref} then the new z_{ref} is obtained by shifting the previous reference point by this increment. The restoring force acting in the dwell phase, *i.e.* when there is no dragging, is equal to $k_z(z - z_{ref})$.

As a result, backtracking no longer takes place. As an unwanted byproduct, this mechanism also prevents the rare events of refolding that have been observed experimentally [67, 68]. The dashed blue line in the top graph of Fig. 8 shows the median t_T in the ratchet model. The times are longer than in the absence of the ratchet in the regime of the larger forces, which is also related to the fact that the distance pulled in one period is restricted. However, translocation still occurs for smaller forces, so it is expected that in the biologically relevant regime of small forces, of order 0.2 ε/Å , the translocation becomes much more efficient.

In the periodic force pulling protocols, proteins may behave

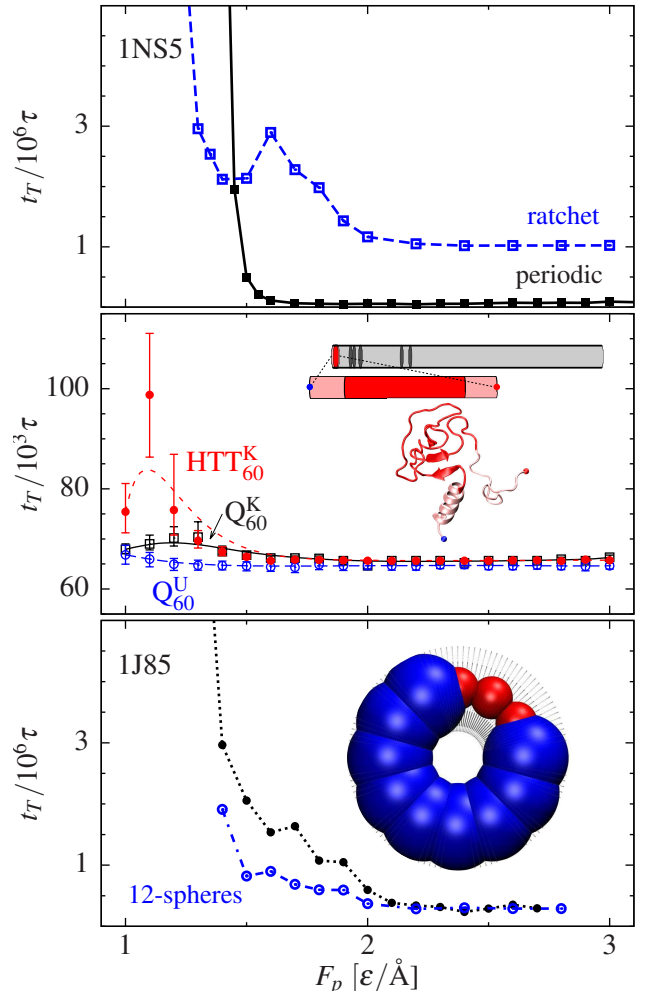


Figure 8: Median translocation time as a function of F_p for different models and systems. The top panel compares periodic pulling with retraction (black solid squares) to the ratchet model (which does not allow for retraction, blue open squares) on 1NS5. The middle panel compares the translocation of knotted and unknotted polyQ conformers (Q_{60}^K in black and Q_{60}^U in blue, respectively) and knotted HTT₆₀ (HTT₆₀^K, in red) translocated using the ratchet model. The inset schematically shows the structure of Huntingtin and its exon 1, where the polyQ region is highlighted in red. The bottom panel shows the difference between the periodic model with a torus entrance (solid black circles) and one with an entrance of 12 spheres of fixed size and a wider cylinder as channel (open blue circles), both of them with backtracking allowed. The inset schematically shows the 12-sphere model, in which three consecutive spheres shrink periodically (highlighted here in red).

in a different manner than in constant speed protocols. Considering, for example, proteins 1J85 and 1NS5, the former jams the proteasome during constant speed, but is degraded in the periodic force protocol while the latter jams the proteasome sometimes (68%) at constant speed, but is slightly worse processed in the periodic force protocol than 1J85, see Fig. 8 – bottom. It is interesting to note that, at least for 1J85, the knot-untying events take place usually during the non-pulling part of the period when the protein attempts to refold.

The ratchet-like pulling model was also applied to Q₆₀ and HTT₆₀, as shown in the middle panel of Fig. 8, which distinguishes between knotted and unknotted conformations. In particular, the optimal pulling force of $2 \text{ } \epsilon/\text{\AA}$ determined for the constant force scenario is preserved in the periodic pulling, even if the effect is much less dramatic in the latter. Furthermore, we observe a maximum similar to the case of 1NS5, but at a lower F_p ($\approx 1.2 \text{ } \epsilon/\text{\AA}$). In any case, the translocation of knotted conformations typically takes more time than the unknotted ones, and is expected to take even longer at low forces, suggesting that the protein degradation machinery might be stalled, or at least hindered, by the knotted conformations.

The 12-sphere model of the entrance to the proteasome

The allosteric action of a proteasome involves not only traction down the channel but also lateral fluctuational changes in the shape of the intake opening [39]. We now address the question of how to incorporate such rotation in a model with an effective potential.

The front ring of the proteasome consists of six proteins with loops that form the entrance to the funnel. These loops undergo allosteric transformations resulting in a bending of the individual loops and in a local deformation of the shape of the entrance. These local deformations are not necessarily consecutive around the entrance – there is a strong random component. However, there appears to be a rotation-like correlation in the events [39]. Our geometrical model may mimic this action by replacing the torus by 12 circularly placed overlapping spheres of radius $6 \text{ } \text{\AA}$ as illustrated in the inset in the bottom panel of Fig. 8. The centers of the spheres are located on a circle of radius R_t (the major radius of the original torus – $13 \text{ } \text{\AA}$). The six loops are meant to be associated with every other sphere. The bending of a loop corresponds to a temporal reduction in the radius of three neighboring spheres to $2 \text{ } \text{\AA}$, after which the radii return to their larger values. For simplicity, we consider the reductions to affect consecutive sets of three spheres and the first sphere of the new set is taken to coincide with the last sphere of the previous set, guaranteeing the aforementioned association of a loop with every other sphere. As a result, the deformation in the shape of the entrance appears to be rotating.

This model requires to expand the cylindrical part of the funnel – the radius of the cylinder is boosted from 8 to $12 \text{ } \text{\AA}$ – to allow for a smooth welding of the two parts of the funnel. Otherwise, a gap between the cylinder and the smaller sphere would form. In the expanded channel, the protein may have enough space to refold. In order to prevent this, we gradually reduce the strength of the protein contacts in the channel to 0 . The molecular motor features of our model include the application of a pulling force F_p combined with the periodic reduction of the radii of three spheres. We take a full period (affecting all spheres consecutively) to be 6000τ – distinct from the 9000τ periodicity of the axial force.

In S6 Fig. we show results for the unknotted protein ADP-ribose pyrophosphatase (with the PDB code 2DSO; studied before in ref. [32]) translocating in the model with the chang-

ing spheres. Compared to the model in which the spheres do not change the radii, the translocation times at low forces get shorter than in the torus-and-cylinder model (by about 84% at an F_p of $1.35 \text{ } \epsilon/\text{\AA}$ and 20% at $1.6 \text{ } \epsilon/\text{\AA}$: the lower the force, the stronger the effect).

The reason for the larger effectiveness is that the unfolding process at the entrance is helped by the time-varying shape of the funnel and translocation is improved by the wider cylinder. We find (by freezing the spheres) that both effects are comparable and become more important as F_p is reduced. However, the enhancement by moving spheres dominates at low forces.

Nonetheless, the rotational mechanism is found not to improve translocation of deeply knotted proteins beyond what the model with non-changing spheres already does. Unlike the smooth funnel model used at constant v_p or F_p , the model with the periodically applied force, with the spheres or without, does allow for both jamming and translocating trajectories for 1J85 in protocol I-C (see bottom panel of Fig. 8). In the periodic models with the fixed-size spheres ($6 \text{ } \text{\AA}$), the median t_T with the narrower cylinder is found to be almost the same as in the smooth-funnel model. On enlarging the cylinder, t_T gets smaller, especially at lower forces. The interesting part is that adding the lateral rotation related to the time-dependent radius of the spheres does not bring any improvement. The reason is that translocation of the knotted proteins does not depend on any additional lateral forces but on the possibility of untying in the idle part of each period. The resulting misfolding during the idle times leads occasionally to the pulled segment to return without threading through the knot-loop, *i.e.* to untying.

The 12-sphere model, especially with the ratchet-like blocking mechanism, is probably the most realistic of the set of models considered here. However, its proper working depends on the adequate choice of the parameters. For instance, when we implement the ratchet mechanism, we impose a condition on the maximum translocation allowed in one period. We take it as $3.8 \text{ } \text{\AA}$, which probably is non-optimal. A greater length may lead to a faster translocation, especially of 1J85 – a process which is not very efficient at low forces. More generally, this length may depend on F_p .

Constant force – all-atom simulations

Fig. 9 shows the results pertaining to pulling 1TIT under protocol II-C using all-atom simulations. In order to neutralize the net charge of $-6 e$ and to have the ionic strength of about 150 mM , we add 64 Na^+ and 58 Cl^- ions. Without the ions, translocation is somewhat faster.

We have focused on two values of F_p : 2.3 and $4.5 \text{ } \epsilon/\text{\AA}$. For larger F_p (such as $15 \text{ } \epsilon/\text{\AA}$) translocation is instantaneous and for $F_p < 2.3 \text{ } \epsilon/\text{\AA}$ there is no forward motion within the time scale of the simulations. After the initial transients, the ratio of the tension at the back terminus to the pulling force is observed to be 0.08 and 0.17 for F_p of 2.3 and $4.5 \text{ } \epsilon/\text{\AA}$ respectively, confirming the mechanical role of the proteasome in defining the conditions of equilibrium. Similar results are obtained for several rotated orientations of the protein about

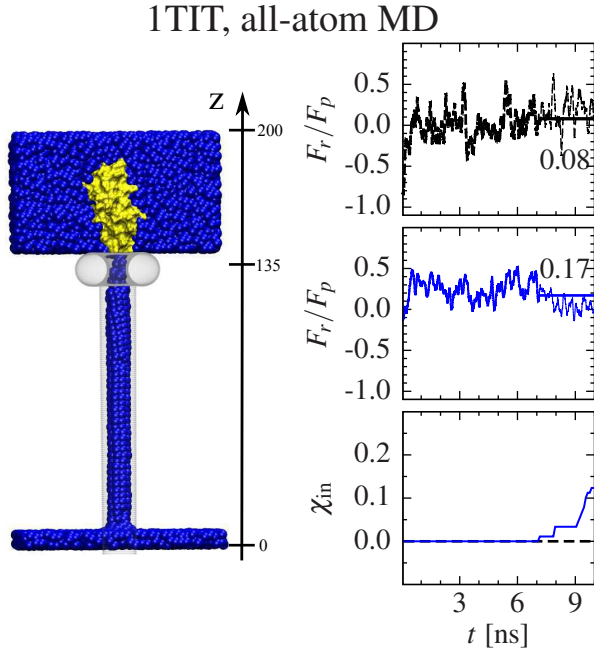


Figure 9: Results of the all-atom simulations for 1TIT. The left section shows the model used for the simulation. At the right, the top and middle panels show the ratio of measured force to applied force when the latter is 2.3 and 4.5 $\epsilon/\text{\AA}$, respectively. The bottom panel shows the fraction of residues that enter the channel as a function of time.

the main axis. At the larger force, about 10% of the residues are seen observed to translocate through the reference plane. Removal of all ions does not affect the tension at the back terminus.

Conclusions

In a previous study [32] we have found that the ease of unfolding and translocation depends on the protein, on the protocol of pulling and on the value of F_p . The same is true in the case of proteins with knots, but the added complexity of such proteins results in either jamming of the proteasome or, at least, an extension of the translocation times significantly. The hindrances are found to grow more and more powerful on lowering F_p to the typical values of the biological motors. The shallowly knotted proteins and the knotted polyQ structures are more likely to hinder the translocation process than to block it, but the hindrances grow rapidly on lowering the pulling force to the biologically relevant regime. On the other hand, the deeply knotted proteins are more likely to jam, especially at small forces (smaller than those used in our simulations) which are relevant biologically. These results, qualitatively, do not depend on the version of the model of the proteasome that is used, even though the timescales do depend on the model. However, the specific outcome depends on the particular model used, for instance, on whether the force is

applied periodically or if the ratchet-like blocking mechanism is built in.

Recently, Szymczak [53, 69] has considered translocation of several knotted proteins through a cylindrical pore connected to a flat plane which is meant to relate to transport through cellular membranes such as the ones in mitochondria. In his model, the interactions with the pore wall are different than in our model but this author has also observed a variety of protein-dependent behaviors when a pulling force was applied and noted that jamming could be avoided by making the force act periodically [70].

On the experimental side, Jackson *et al.* have considered knotted proteins 1XD3 and 1NS5 in ClpP/X assays and also found a rich variety in their behavior (personal communication). 1NS5 entering through the C-terminus degrades rapidly, consistent with our results with the periodic force, unless a stable ThiS domain is attached at the N-terminus. On the other hand, 1XD3 is resistant to degradation in what we call protocol I-C. This is surprising because the N-terminal knot is shallow and should untie readily as we find in the constant-speed case.

Specifically in the case of neurodegeneration, our work shows how knotted polyglutamine tracts hinder the proteasomal function both when isolated and when flanked by one of the naturally occurring flanking sequences, huntingtin exon 1. An inefficient degradation may unbalance the concentration of elements to degrade in the cell, which might be related to toxicity in two ways: the accumulation of monomers will increase the probability of one of them becoming toxic; and the enhanced number of molecules will increase the concentration of the neurotoxic proteins, which will then aggregate into toxic oligomers after the critical concentration of the process is reached. Both mechanisms of toxicity suggested for polyglutamine differ from the proposed effect of metals, such as copper and zinc [71–74] in the aggregation of α -synuclein or β -amyloid. This marks an important difference between the genetically determined diseases (polyglutaminopathies such as Huntington) compared to environmentally driven ones (like the sporadic form of Alzheimer or Parkinson).

There has been considerable debate about the role of knots in proteins in general. One possible role is to enhance the mechanical, kinetic, and thermodynamic stability of a protein [75]. Here, we have investigated a harmful role: reduction in the efficiency or even derailing of the protein degradation process, which may result in toxicity.

Acknowledgments

We appreciate stimulating discussions with S. E. Jackson, M. Sikora, R. Hervás and K. Wołek. We also acknowledge the contribution of SVG High-Performance Computing facility provided by the Galician Supercomputing Center (CESGA), www.cesga.es. This work has been supported by the EU Joint Programme in Neurodegenerative Diseases project (JPND CD FP-688-059). The project is supported through the following funding organisations under the aegis of JPND - www.jpnd.eu: Ireland, HRB; Poland, National

Science Centre (2014/15/Z/NZ1/00037); and Spain, ISCIII (AC14/00037 ISCIII). MW has been supported by Polish Na-

tional Science Centre Grant No. 2014/15/B/ST3/01905. AGS was supported by a JAE doctoral fellowship from CSIC.

- [1] V. K. Mulligan and A. Chakraborty, *Proteins Struct Funct Bioinf*, 2013, **81**, 1285–1303.
- [2] M. R. Sawaya, S. Sambashivan, R. Nelson, M. I. Ivanova, S. A. Sievers, M. I. Apostol, M. J. Thompson, M. Balbirnie, J. J. Wiltzius, H. T. McFarlane et al., *Nature*, 2007, **447**, 453–457.
- [3] R. Kaye, E. Head, J. L. Thompson, T. M. McIntire, S. C. Milton, C. W. Cotman and C. G. Glabe, *Science*, 2003, **300**, 486–489.
- [4] R. Hervás, J. Oroz, A. Galera-Prat, O. Goñi, A. Valbuena, A. M. Vera, A. Gómez-Sicilia, F. Losada-Urzáiz, V. N. Uversky, M. Menéndez, D. V. Laurents, M. Bruix and M. Carrión-Vázquez, *PLoS Biol*, 2012, **10**, e1001335.
- [5] A. C. M. Ferreol, C. R. Moran, Y. Gambin and A. A. Deniz, *Methods Enzymol*, 2010, **472**, 179–204.
- [6] A. Gómez-Sicilia, M. Sikora, M. Cieplak and M. Carrión-Vázquez, *PLoS Comput Biol*, 2015, **11**, e1004541.
- [7] P. Cossio, A. Trovato, F. Pietrucci, F. Seno, A. Maritan and A. Laio, *PLoS Comput Biol*, 2010, **6**, e1000957.
- [8] I. Sillitoe, A. L. Cuff, B. H. Dessailly, N. L. Dawson, N. Furnham, D. Lee, J. G. Lees, T. E. Lewis, R. A. Studer, R. Rentzsch, C. Yeats, J. M. Thornton and C. A. Orengo, *Nucleic Acids Res*, 2013, **41**, D490–D498.
- [9] M. Jamroz, W. Niemyska, E. J. Rawdon, A. Stasiak, K. C. Millett, P. Sułkowski and J. I. Sułkowska, *Nucleic Acids Res*, 2015, **43**, D306–D314.
- [10] P. Virnau, L. A. Mirny and M. Kardar, *PLoS Comput Biol*, 2006, **2**, e122.
- [11] S. a Beccara, T. Škrbić, R. Covino, C. Micheletti and P. Faccioli, *PLoS Comput Biol*, 2013, **9**, e1003002.
- [12] J. K. Noel, J. N. Onuchic and J. I. Sułkowska, *J Phys Chem Lett*, 2013, **4**, 3570–3573.
- [13] M. Chwastyk and M. Cieplak, *J Chem Phys*, 2015, **143**, 045101.
- [14] H. M. Berman, J. Westbrook, Z. Feng, G. Gilliland, T. N. Bhat, H. Weissig, I. N. Shindyalov and P. E. Bourne, *Nucleic Acids Res*, 2000, **28**, 235–242.
- [15] P. Virnau, A. Mallam and S. Jackson, *J Phys Condens Matter*, 2011, **23**, 033101.
- [16] J. I. Sułkowska, E. J. Rawdon, K. C. Millett, J. N. Onuchic and A. Stasiak, *Proc Natl Acad Sci USA*, 2012, **109**, E1715–E1723.
- [17] N. C. H. Lim and S. E. Jackson, *J Phys Condens Matter*, 2015, **27**, 354101.
- [18] R. Konrat, *Biophys J*, 2015, **109**, 1309–1311.
- [19] J. Nasir, S. B. Floresco, J. R. O’Kusky, V. M. Diewert, J. M. Richman, J. Zeisler, A. Borowski, J. D. Marth, A. G. Phillips and M. R. Hayden, *Cell*, 1995, **81**, 811–823.
- [20] C. Zuccato, A. Ciammola, D. Rigamonti, B. R. Leavitt, D. Goffredo, L. Conti, M. E. MacDonald, R. M. Friedlander, V. Silani, M. R. Hayden, T. Timmusk, S. Sipione and E. Cattaneo, *Science*, 2001, **293**, 493–498.
- [21] J. Velier, M. Kim, C. Schwarz, T. W. Kim, E. Sapp, K. Chase, N. Aronin and M. DiFiglia, *Exp Neurol*, 1998, **152**, 34–40.
- [22] J. Petruska, M. J. Hartenstine and M. F. Goodman, *J Biol Chem*, 1998, **273**, 5204–5210.
- [23] S. C. Warby, H. Visscher, J. A. Collins, C. N. Doty, C. Carter, S. L. Butland, A. R. Hayden, I. Kanazawa, C. J. Ross and M. R. Hayden, *Eur J Hum Genet*, 2011, **19**, 561–566.
- [24] M. DiFiglia, E. Sapp, K. O. Chase, S. W. Davies, G. P. Bates, J. P. Vonsattel and N. Aronin, *Science*, 1997, **277**, 1990–1993.
- [25] M. Verma, A. Vats and V. Taneja, *Ann Indian Acad Neurol*, 2015, **18**, 138–145.
- [26] C. A. Ross and M. A. Poirier, *Nat Med*, 2004, **10 Suppl**, S10–S17.
- [27] Y. Nagai, T. Inui, H. A. Popiel, N. Fujikake, K. Hasegawa, Y. Urade, Y. Goto, H. Naiki and T. Toda, *Nat Struct Mol Biol*, 2007, **14**, 332–340.
- [28] N. F. Bence, R. M. Sampat and R. R. Kopito, *Science*, 2001, **292**, 1552–1555.
- [29] Koniaris and Muthukumar, *Phys Rev Lett*, 1991, **66**, 2211–2214.
- [30] W. R. Taylor, *Nature*, 2000, **406**, 916–919.
- [31] M. Chwastyk and M. Cieplak, *J Phys Condens Matter*, 2015, **27**, 354105.
- [32] M. Wojciechowski, P. Szymczak, M. Carrión-Vázquez and M. Cieplak, *Biophys J*, 2014, **107**, 1661–1668.
- [33] O. Cux, K. Tanaka and A. L. Goldberg, *Annu Rev Biochem*, 1996, **65**, 801–847.
- [34] A. L. Goldberg, *Semin Cell Biol*, 1990, **1**, 423–432.
- [35] S. Gottesman, *Annu Rev Genet*, 1996, **30**, 465–506.
- [36] F. Zhang, M. Hu, G. Tian, P. Zhang, D. Finley, P. D. Jeffrey and Y. Shi, *Mol Cell*, 2009, **34**, 473–484.
- [37] M. Groll, L. Ditzel, J. Löwe, D. Stock, M. Bochtler, H. D. Bartunik and R. Huber, *Nature*, 1997, **386**, 463–471.
- [38] A. Kravats, M. Jayasinghe and G. Stan, *Proc Natl Acad Sci USA*, 2011, **108**, 2234–2239.
- [39] S. Tonddast-Navaei and G. Stan, *J Am Chem Soc*, 2013, **135**, 14627–14636.
- [40] A. N. Kravats, S. Tonddast-Navaei, R. J. Bucher and G. Stan, *J Chem Phys*, 2013, **139**, 121921.
- [41] R. A. Maillard, G. Chistol, M. Sen, M. Righini, J. Tan, C. M. Kaiser, C. Hodges, A. Martin and C. Bustamante, *Cell*, 2011, **145**, 459–469.
- [42] M.-E. Aubin-Tam, A. O. Olivares, R. T. Sauer, T. A. Baker and M. J. Lang, *Cell*, 2011, **145**, 257–267.
- [43] T. X. Hoang and M. Cieplak, *J Chem Phys*, 2000, **112**, 6851–6862.
- [44] M. Cieplak and T. X. Hoang, *Biophys J*, 2003, **84**, 475–488.
- [45] J. I. Sułkowska and M. Cieplak, *J Phys Condens Matter*, 2007, **19**, 283201.
- [46] J. I. Sułkowska and M. Cieplak, *Biophys J*, 2008, **95**, 3174–3191.
- [47] M. Sikora, J. I. Sułkowska and M. Cieplak, *PLoS Comput Biol*, 2009, **5**, e1000547.
- [48] M. Muthukumar, *Annu Rev Biophys Biomol Struct*, 2007, **36**, 435–450.
- [49] S. Kirmizialtin, V. Ganesan and D. E. Makarov, *J Chem Phys*, 2004, **121**, 10268–10277.
- [50] L. Huang, S. Kirmizialtin and D. E. Makarov, *J Chem Phys*, 2005, **123**, 124903.
- [51] D. K. West, D. J. Brockwell and E. Paci, *Biophys J*, 2006, **91**, L51–L53.
- [52] D. E. Makarov, *Acc Chem Res*, 2009, **42**, 281–289.
- [53] P. Szymczak, *Biochem Soc Trans*, 2013, **41**, 620–624.
- [54] P. Tian and I. Andricioaei, *J Mol Biol*, 2005, **350**, 1017–1034.

- [55] N. Go, Annu Rev Biophys Bioeng, 1983, **12**, 183–210.
- [56] S. Takada, Proc Natl Acad Sci U S A, 1999, **96**, 11698–11700.
- [57] K. Wołek, A. Gómez-Sicilia and M. Cieplak, J Chem Phys, 2015, **143**, 243105.
- [58] A. Galera-Prat, A. Gómez-Sicilia, A. F. Oberhauser, M. Cieplak and M. Carrión-Vázquez, Curr Opin Struct Biol, 2010, **20**, 63–69.
- [59] N. Eswar, B. Webb, M. A. Marti-Renom, M. S. Madhusudhan, D. Eramian, M.-Y. Y. Shen, U. Pieper and A. Sali, in Comparative protein structure modeling using Modeller, John Wiley & Sons, Inc., 2006, ch. 5.
- [60] M. W. Kim, Y. Chelliah, S. W. Kim, Z. Otwinowski and I. Bezprozvanny, Structure, 2009, **17**, 1205–1212.
- [61] D. Van Der Spoel, E. Lindahl, B. Hess, G. Groenhof, A. E. Mark and H. J. C. Berendsen, J Comput Chem, 2005, **26**, 1701–1718.
- [62] E. J. Sorin and V. S. Pande, Biophys J, 2005, **88**, 2472–2493.
- [63] W. L. Jorgensen, J. Chandrasekhar, J. K. Buckner and J. D. Madura, Ann N Y Acad Sci, 1986, **482**, 198–209.
- [64] W. Humphrey, A. Dalke and K. Schulten, J Mol Graphics, 1996, **14**, 33–38.
- [65] P. Szymczak and M. Cieplak, Journal of Physics: Condensed Matter, 2005, **18**, L21.
- [66] J. I. Sułkowska, P. Sułkowski, P. Szymczak and M. Cieplak, Phys Rev Lett, 2008, **100**, 058106.
- [67] M. Sen, R. A. Maillard, K. Nyquist, P. Rodriguez-Aliaga, S. Pressé, A. Martin and C. Bustamante, Cell, 2013, **155**, 636–646.
- [68] M. R. Maurizi and G. Stan, Cell, 2013, **155**, 502–504.
- [69] P. Szymczak, The European Physical Journal Special Topics, 2014, **223**, 1805–1812.
- [70] P. Szymczak, Sci Rep, 2016, **6**, 21702.
- [71] P. Zatta, D. Drago, S. Bolognin and S. L. Sensi, Trends Pharmacol Sci, 2009, **30**, 346–355.
- [72] H. Kozłowski, M. Luczkowski, M. Remelli and D. Valensin, Coordination Chemistry Reviews, 2012, **256**, 2129–2141.
- [73] Y. Miller, B. Ma and R. Nussinov, Coordination Chemistry Reviews, 2012, **256**, 2245–2252.
- [74] J. H. Viles, Coordination Chemistry Reviews, 2012, **256**, 2271–2284.
- [75] J. I. Sułkowska, P. Sułkowski, P. Szymczak and M. Cieplak, Proc Natl Acad Sci USA, 2008, **105**, 19714–19719.